

TRAP DENSITY IMAGING OF SILICON WAFERS USING A LOCK-IN INFRARED CAMERA TECHNIQUE

Peter Pohl, Jan Schmidt, Karsten Bothe, and Rolf Brendel
Institut für Solarenergieforschung Hameln (ISFH), Am Ohrberg 1, D-31850 Emmerthal, Germany

ABSTRACT

We apply a novel an imaging technique for non-recombination active minority-carrier trapping centres in silicon wafers based on lock-in infrared thermography. Measurements on Czochralski silicon wafers show that the trap density is highly inhomogenous and correlates with oxygen-induced striation patterns. A direct comparison of the trap density image with the corresponding recombination lifetime mapping reveals an anticorrelation of the two quantities. The application of the ITM technique to block-cast multicrystalline silicon wafers shows that the distribution of the trapping centres correlates with the dislocation density. Moreover, we find that areas with increased dislocation density often degrade during phosphorus gettering treatment. Finally, we demonstrate that one single spatially resolved measurement of the infrared emission signal of as-delivered multicrystalline silicon without surface passivation layers reveals already poorly-getterable areas, which decrease the solar cell efficiency. Hence, trap density imaging is a useful new instrument for assessing the efficiency potential of as-delivered mc-Si wafers.

INTRODUCTION

In block-cast multicrystalline silicon (mc-Si) and monocrystalline Czochralski silicon (Cz-Si) abnormally high lifetimes are frequently measured when minority-carrier trapping centres are present in a significant concentration [1-3]. The high apparent lifetimes obtained from photoconductance-based measurement techniques at low injection levels should not be confused with the actual recombination lifetime [2]. At excess carrier concentrations comparable to or below the trap density charge neutrality implies that the presence of minority-carrier traps causes a relative increase in the concentration of majority carriers, leading to an increase in the steady-state photoconductance [2].

The physical origins of minority-carrier trapping centres in silicon wafers seem to be manifold and are not well understood up to now. Recently, Macdonald et al. [4] showed that in boron-doped mc-Si at least two different types of traps may be present. One species can be removed by phosphorus gettering and is related to the presence of boron-related centres. The other type is impervious to gettering and is correlated to the dislocation density. In Cz-Si wafers, a clear correlation of the trap density with the oxygen content and the doping concentration has been found [3]. This finding led to the conclusion that the

minority-carrier trapping centres in Cz-Si are oxygen-related defects.

In this paper, we use the Infrared Trap Mapping (ITM) technique [5], which is deduced from the Infrared Lifetime Mapping [ILM, also known as CDI] technique introduced by Bail et al. [6-8]. ITM enables us to image trap densities as well as energy levels of traps in semiconductors [5]. We apply the method to Cz-Si as well as mc-Si wafers. Moreover, the influence of the trapping centres in mc-Si on solar cell properties is studied.

EXPERIMENTAL

In our experimental setup (Fig. 1), an infrared camera that is sensitive in the long-wavelengths range [peak sensitivity at a wavelength of $\lambda_{\text{det}} = (8.3 \pm 0.6) \mu\text{m}$, frame rate 38.9 Hz, focal plane array with 640×486 detectors] images the infrared emission intensity of the semiconductor wafer that is heated to a constant temperature T_w in the range of 20-150°C. Our currently used optical setup allows for a spatial resolution of 200 μm . In order to extract the injection-dependent lifetimes, we generate excess carriers in the silicon wafer by means of an LED array ($\lambda_{\text{ex}} = 880 \text{ nm}$), which is periodically turned on and off. The photon flux is measured by a calibrated solar cell. The emission change at $\lambda_{\text{det}} = 8.3 \mu\text{m}$ is determined using lock-in technique as described by Breitenstein and Langenkamp [9]. We apply a low lock-in frequency (typically 0.1 - 2 Hz). Hence, the in-phase camera signal S_0 is used to calculate the lifetime since the excess carrier concentration is in phase with the illumination intensity. As our measurements are performed under steady-state conditions, we determine the apparent lifetime τ_a of the sample using the simple expression [8]

$$\tau_a = \frac{S_0}{m(1 + \alpha_n/\alpha_p)gW}, \quad (1)$$

where g denotes the photogeneration rate of electron-hole pairs and W the thickness of the sample. m is a proportionality factor, which has been measured using a set of p -type silicon wafers of different well-defined doping concentrations. Details of the calibration procedure were described elsewhere [8]. The correction factor $(1 + \alpha_n/\alpha_p)$ includes the absorption coefficient for electrons α_n and holes α_p at the detection wavelength λ_{det} and accounts for the fact that under illumination electrons as well as holes are generated, whereas in our calibration procedure only

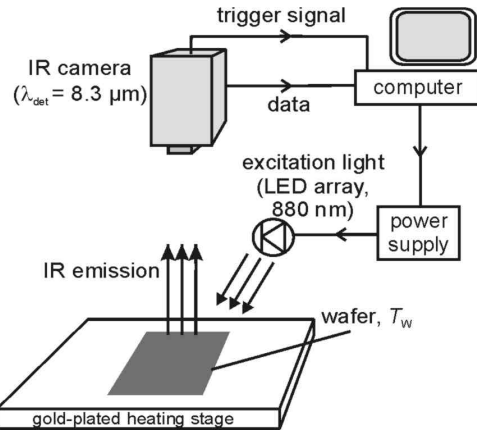


Fig. 1. Experimental setup: The wafer is heated to a temperature T_w by a gold-plated heater with low emissivity. The modulated excitation light causes a modulated infrared emission by photogenerated free carriers that is observed by the IR camera.

p -type material is used [10]. According to Kirchhoff's law, the absorption coefficient always equals the emission coefficient $\alpha(\lambda) = \varepsilon(\lambda)$. Hence, the measurement can be performed in absorption or emission mode, depending on the temperature of the material under investigation and the temperature of the background. In this paper, we measure in emission mode at a sample temperature of 70°C .

Using an automated fitting routine based on the downhill simplex algorithm [11], we apply a single-level trap model introduced by Hornbeck and Haynes [12] to the experimental data in order to calculate the local densities and ionization energies of the trapping centres. The apparent lifetime for p -type material is given by the expression [5]

$$\tau_a = \tau_t \left(1 + \frac{N_t}{\Delta n + N_t} \frac{\tau_t}{\tau_d} \frac{\alpha_p}{\alpha_p + \alpha_n} \right), \quad (2)$$

where τ_t is the recombination lifetime, N_t the trap density and τ_t/τ_d the ratio of trapping-to-detraping time constants. For n -type material, α_p in the nominator has to be replaced by α_n . As our measurements are performed under low-level injection conditions, τ_t does not depend on the injection level. Furthermore, the apparent carrier concentration Δn_a is related to the actual excess carrier concentration Δn via $\Delta n_a = \tau_a/\tau_t \times \Delta n$.

Space charge regions due to interior or exterior interfaces in the sample can cause a similar effect as described by the Hornbeck-Haynes model. We will introduce a model dealing with the modulation of space charge regions forming around structural defects in silicon in a separate contribution [13: to be published].

APPLICATION TO CZOCHRALSKI SILICON

We apply the ITM technique to Cz-Si wafers. Both wafer surfaces are passivated with 70 nm thick silicon nitride (SiN_x) films deposited in a remote plasma-enhanced chemical vapor deposition system at 400°C .

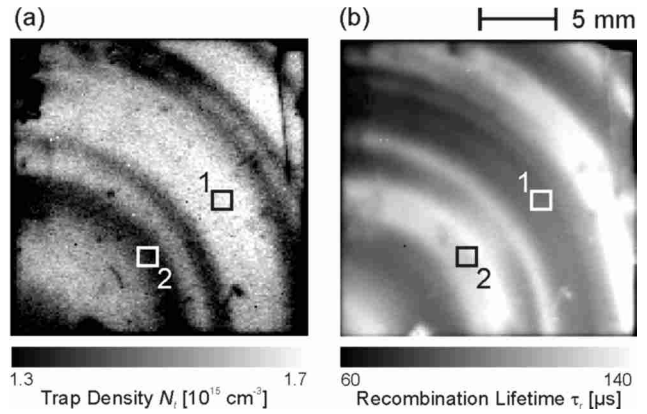


Fig. 2. a) Trap density mapping of a Cz-Si wafer measured by ITM. b) Recombination lifetime mapping of the same sample measured by ILM. A clear anticorrelation between the trap density and the recombination lifetime mapping is found.

Fitting Eq. (2) to the experimental data $\tau_a(\Delta n_a)$ results in the N_t image shown in Fig. 2a. The trap density $N_t(x,y)$ ranges from 1.3 to $1.7 \times 10^{15} \text{ cm}^{-3}$. The area-averaged trap density is $\langle N_t \rangle = (1.53 \pm 0.11) \times 10^{15} \text{ cm}^{-3}$. It is interesting to note that, as can be seen from Fig. 2a, there exists a correlation between the trap density and striation patterns, which are caused by a variation of the oxygen content [14]. Also, a clear anticorrelation between the trap density in Fig. 2a and the recombination lifetime mapping in Fig. 2b is found. Due to the fact that some oxygen-related defects (e.g. oxygen precipitates) (ODs) are known as strong recombination centres, we assume that areas with increased τ_r (position 2 in Fig. 2b) exhibit a lower concentration of ODs and vice versa (position 1). Hence, areas with an increased N_t correlate to areas with an increased concentration of ODs. However, it remains unclear, whether the ODs themselves or secondary defects generated in the stress field of the ODs are the reason for the increased trap density N_t .

An image of the trap energy level E_t (calculated according to Ref. 5, Eq. (7)) reveals a homogeneous distribution around $E_t = E_v + (0.587 \pm 0.005) \text{ eV}$. The homogeneity in E_t over the measured area is better than 1%, whereas the homogeneity in N_t is $\sim 7\%$, suggesting that only one type of trap is measured. It has been shown recently that oxygen-related traps can be present in large concentrations in Cz-Si [3]. The fact that the energy level of the trapping center is very deep is surprising at first glance. One reason might be that the deep traps are heavily charged, repelling majority carriers and therefore having only little recombination activity. However, the deepness of the traps might also be a result of the oversimplification of the trap model [3].

APPLICATION TO MULTICRYSTALLINE SILICON

As-grown state

Figure 3 shows two lifetime images $\tau_a(x,y)$ of the same mc-Si sample at two different illumination intensities (3×10^{-3} suns and 1 sun). Due to minority-carrier trapping,

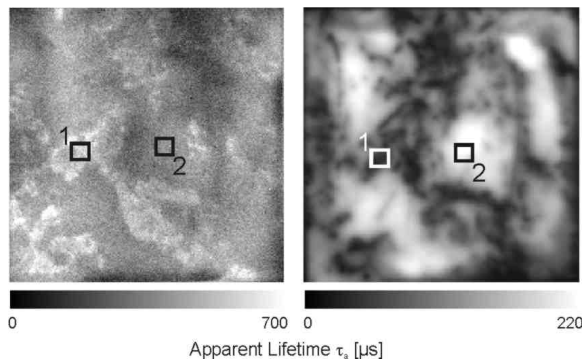


Fig. 3. Apparent lifetime images $\tau_a(x,y)$ of a mc-Si wafer obtained from lock-in infrared emission measurements at 70°C. The mappings are measured at two different illumination intensities: (a) 3×10^{-3} suns and (b) 1 sun.

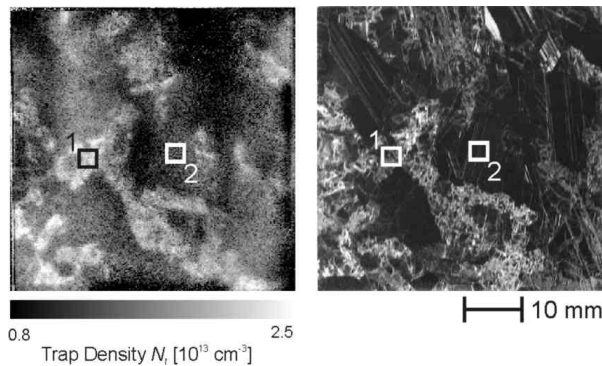


Fig. 4. (a) Trap density image $N_t(x,y)$ of the mc-Si wafer shown in Fig. 3. (b) Scanned picture of the same wafer after removal of the silicon nitride passivation layers and application of a Dash [15] etch. Brighter regions correspond to areas of increased dislocation densities.

under low-injection conditions the area-averaged lifetime in Fig. 3a of $\tau_a = 350 \mu\text{s}$ is much larger than the area-averaged lifetime of $\tau_a = 110 \mu\text{s}$ at 1 sun (Fig. 3b), where trapping effects are negligible and thus the actual recombination lifetime is measured. As can be seen from Fig. 3, the two lifetime mappings do not correlate. Apparently, additional information is provided by the lifetime image measured at an illumination intensity of 3×10^{-3} suns.

Fitting Eq. (2) to the experimental data results in the N_t image shown in Fig. 4a. The obtained N_t image does not correlate with the grain structure of the wafer. Thus, we applied a Dash etch [15] for 3h to reveal a possible correlation with structural defects, especially dislocations. Indeed, the spatial distribution of dislocations shown in Fig. 4b is in excellent agreement with the distribution of N_t (Fig. 4a). The brighter regions in Fig. 4b correspond to areas of increased dislocation densities. These regions correlate well with the areas of increased trap densities N_t (Fig. 4a).

Impact of phosphorus gettering

Subsequent to the application of a phosphorus-gettering treatment at 850°C using POCl_3 we measure the wafers again (after removing the diffused n^+ -regions and passivating both surfaces with SiN_x). A comparison of the recombination lifetime determined at an injection density

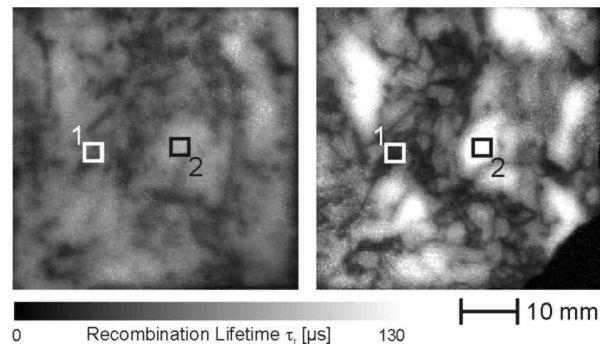


Fig. 5. Recombination lifetime images $\tau_r(x,y)$ determined at an injection density level of $\Delta n = 10^{14} \text{ cm}^{-3}$ as calculated by an automated fitting routine based on a single-level trap model for the wafer shown in Fig. 3 before (a) and after (b) a phosphorus gettering.

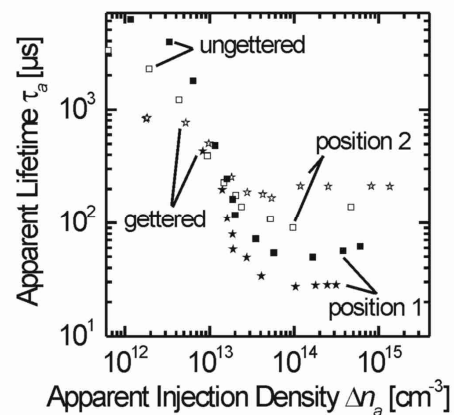


Fig. 6. Injection-dependent lifetime curves $\tau_a(\Delta n_a)$ at two different positions (marked in Figs. 3-5) of a mc-Si wafer obtained from lock-in infrared emission measurements. The wafer was measured before (squares) and after (stars) phosphorus gettering at 850°C.

of $\Delta n = 10^{14} \text{ cm}^{-3}$ before and after gettering is shown in Fig. 5. The area-averaged lifetime increases from $\langle \tau_r \rangle = 51.9 \mu\text{s}$ before gettering to $\langle \tau_r \rangle = 65.3 \mu\text{s}$ after gettering. Moreover, one can clearly see that τ_r increases in particular in those regions, which already had the highest lifetimes before gettering. In regions of relatively low lifetimes before gettering, the recombination lifetime shows a reduced improvement or even decreases.

Figure 6 shows injection-dependent lifetime curves $\tau_a(\Delta n_a)$ measured at the two different positions on the wafer indicated in Figs. 3-5. The two positions correspond to areas with highest and lowest trap densities. At position 1, we measure $N_t = 2.06 \times 10^{13} \text{ cm}^{-3}$ and at position 2, $N_t = 0.90 \times 10^{13} \text{ cm}^{-3}$. The injection-dependent lifetime curves in Fig. 6 show that for the highest measured injection densities above $1 \times 10^{14} \text{ cm}^{-3}$, trapping effects are negligible and, thus, the actual recombination lifetime is measured. The curve measured at position 2 clearly reveals an increase of the recombination lifetime after gettering, whereas at position 1, τ_r decreases after the phosphorus gettering treatment.

Our interpretation of the observed behavior is that areas exhibiting higher dislocation densities (position 1) contain significant concentrations of impurities (e.g., metals), which are restrained in the stress field of the dislocations. These impurities are set free during the high-temperature gettering treatment and contaminate the surrounding region. This effect may lead to a severe degradation in the solar cell performance in contrast to regions with lower dislocation densities (position 2), where the phosphorus gettering treatment mainly removes recombination-active metallic impurities.

TRAP MAPPING WITHOUT SURFACE PASSIVATION

As already mentioned in the previous Section, the apparent lifetime image (Fig. 3a) and the corresponding N_t image (Fig. 4a) show a good qualitative agreement, demonstrating that a single ILM measurement already reveals if trapping at dislocations is present and which regions of the wafer are affected. In order to proof a possible industrial applicability of our novel trap mapping technique using an infrared camera, we perform only one single IR emission measurement on as-delivered mc-Si wafers without applying any surface treatment. Figure 7a shows the measured infrared emission picture $S_0(x,y)$ of an as-grown block-cast mc-Si wafer from Photowatt ($125 \times 125 \text{ mm}^2$) recorded at 1/100 suns. The measurement period was 20 min. The image reveals areas with increased dislocation densities located on the left-hand side, bottom side and top right corner of the wafer. A comparison with the N_t image (Fig. 7b) reveals good correlation between the two images.

As mentioned in the previous Section, we expect that regions of increased dislocation densities correlate with increased densities of metallic impurities, partly in the form of nano precipitates. A high-temperature step such as the phosphorus gettering may lead to a severe lifetime degradation within such areas. The detection of those regions might be used to estimate the contribution of poorly-getterable areas of the wafer, which decrease the solar cell efficiency.

Hence, we conclude that the application of a spatially resolved measurement using an IR camera helps to identify poorly-getterable areas in as-delivered mc-Si wafers without the need of any surface treatment.

CONCLUSIONS

We have applied the novel Infrared Trap Mapping (ITM) technique, which enables one to image absolute values of densities and energy levels of minority-carrier trapping centres in semiconductors. Application of the method to **Cz-Si** indicated that the ITM technique detects either oxygen-related precipitates or secondary defects generated in the stress field of the oxygen-related precipitates, whereas the recombination lifetime mappings reveal areas of increased recombination due to the oxygen-related precipitates. Our measurements on block-cast mc-Si wafers revealed a strong correlation between regions with increased trap densities and areas with increased dislocation densities. Areas with an increased dislocation density showed a strong deterioration of the recombination lifetime after phosphorus gettering. These regions have a significant impact on the recombination

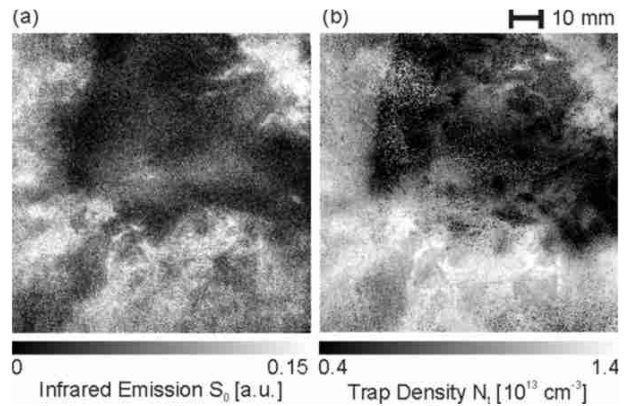


Fig. 7. (a) Infrared emission signal $S_0(x,y)$ of a block-cast mc-Si wafer without any surface treatment measured at an illumination intensity of 0.01 suns. Brighter regions correspond to areas of increased trap densities. (b) Trap density image $N_t(x,y)$ of the same wafer after passivating both surfaces with SiN_x .

lifetime at relevant injection levels for solar cells and, thus, have a significant impact on solar cell device performance. Finally, we have demonstrated that one single spatially resolved measurement of the infrared emission signal of as-delivered multicrystalline silicon without any surface treatment reveals already poorly-getterable areas, which decrease the solar cell efficiency. Hence, we conclude that a detailed information of the trap density in the as-grown silicon material is – besides the recombination lifetime – a crucial material parameter for the comprehensive assessment of the efficiency potential of mc-Si wafers.

Acknowledgements

Funding was provided by the State of Lower Saxony. The authors are grateful to N. Enjalbert of Photowatt International S.A.S (France) for supplying mc-Si wafers. ISFH is a member of the German Forschungsverbund Sonnenenergie.

REFERENCES

- [1] R. Bube, *Photoelectronic Properties of Semiconductors* (Cambridge, UK, 1992).
- [2] D. Macdonald, A. Cuevas, *Appl. Phys. Lett.* **74**, 1710 (1999).
- [3] J. Schmidt, K. Bothe, R. Hezel, *Appl. Phys. Lett.* **80**, 4395 (2002).
- [4] D. Macdonald A. Cuevas, *Solar Energy Materials & Solar Cells*, **65**, 509 (2001).
- [5] P. Pohl, J. Schmidt, K. Bothe, and R. Brendel, *Appl. Phys. Lett.* **87**, 142104 (2005).
- [6] M. Bail, J. Kentsch, R. Brendel, and M. Schulz, in *Proc. of the 28th IEEE Photovoltaics Conference* (Anchorage, 2000), pp. 99-101.
- [7] S. Riepe, J. Isenberg, C. Balif, S. W. Glunz, W. Warta, in *Proc 17th European Photovoltaic Solar Energy Conf. (Munich, 2001)*, p. 1597.
- [8] P. Pohl, R. Brendel, in *Proc. 19th European Photovoltaic Solar Energy Conference* (Paris, 2004), pp. 46-49.
- [9] O. Breitenstein, M. Langenkamp, *Lock-in thermography* (Springer Verlag, 2003).
- [10] D. Schroder, R. Thomas, J. Schwartz, *IEEE Trans. Electron Devices* **25**, 254 (1978).
- [11] W.H. Press, S.A. Teukolsky, W.T. Vetterling, and B.P. Flannery, *Numerical Recipes in C* (Cambridge University Press, 1999).
- [12] J. Hornbeck and J. Haynes, *Phys. Rev.* **97**, 311 (1955).
- [13] P. Pohl et al., to be published.
- [14] I. Fusegawa and H. Yamagishi, *Semicond. Sci. Technol.* **7**, 304 (1992).
- [15] W.C. Dash, *J. Appl. Phys.* **27**, 1193 (1957).